RSC Advances

PAPER

View Article Online
View Journal | View Issue

Cite this: *RSC Adv.*, 2022, **12**, 4408

Embedded ionic liquid modified ZIF-8 in CaMgAl hydrotalcites for bio-glycerol transesterification†

Guanhao Liu, Jingyi Yang,* Yibo Zhao and Xinru Xu*

Novel modified MOF intercalated hydrotalcites was synthesized for catalyzing the conversion of glycerol into high value-added glycerol carbonate in this paper. [APmim]OH/ZIF-8 was prepared by encapsulating aminopropyl hydroxide imidazole ionic liquid in ZIF-8 and inserted in Ca–Mg–Al hydrotalcites with layered structures to prepare [APmim]OH/ZIF-8/LDH with strong basicity and high specific surface area. ZIF-8, [APmim]OH/ZIF-8 and [APmim]OH/ZIF-8/LDH were characterized by XRD, FT-IR, SEM and nitrogen adsorption–desorption. The results showed that the conversion rate of glycerol can reach 98.6% and the glycerol carbonate yield was 96.5% in the transesterification of glycerol with dimethyl carbonate catalyzed by [APmim]OH/ZIF-8/LDH when the molar ratio of DMC and glycerol was 3 : 1, the catalyst dosage was 3 wt%, the reaction temperature was 75 °C and the reaction time was 80 minutes. The glycerol conversion rate can still reach more than 90% after five reaction cycles.

Received 8th December 2021
Accepted 17th January 2022

DOI: 10.1039/d1ra08928e

rsc.li/rsc-advances

1 Introduction

Glycerol carbonate (GC) is one of the most promising derivatives in glycerol derivatives.[1–4] GC was widely used in original solvents, elastomers, surfactants, adhesives, inks, paints, lubricants due to its remarkable biodegradability, water solubility, low viscosity, low toxicity and high boiling point.[5–7] Moreover, GC molecules contain different functional groups, which show high reactivity with alcohols, amines, carboxylic acids, ketones and isocyanates.

The transesterification of glycerol with DMC over basic catalysts was considered to be an effective method for the synthesis of GC under mild conditions.[8] This reaction avoided toxic substances, high pressure and other harsh conditions compared with other reaction routes.[9,10] The glycerol conversion and GC yield in this reaction mainly depended on the basic sites and base density on the catalyst. Excessive alkaline strength (H_>26.5) can cause GC decomposition to generate glycidol.[11]

Ionic liquids as green catalysts can be designed and synthesized according to service conditions.[12–14] The use of basic ionic liquids in transesterification is conducive to sustainable development and environmental protection. However, ionic liquids are not suitable for industrial applications since they are not easily separated and recovered in reaction systems.[15] Thus it is significant to find suitable carriers to prepare heterogeneous catalysts with strong catalytic activity, high stability and easy recyclability in transesterification between glycerol and DMC to prepare GC.[16,17]

Metal organic framework materials (MOFs) are coordination polymers with three-dimensional pore structures.[18] Metal ions in MOFs usually serve as connection points and organic ligands support the spatial extension. MOFs have become a prominent research direction in many chemical embranchment subjects as another important novel porous material besides zeolites and carbon nanotubes.[19] Zeolitic imidazole framework-8 (ZIF-8) self-assembled by coordination of zinc ions and 2-methylimidazole has been widely used in catalysis, energy storage and separation due to its outstanding advantages such as large surface area, high porosity, convenient synthesis and controllable size.[20,21]

The basicity strength of ZIF-8 can be greatly increased by modification of basic ionic liquids, which was beneficial for the transesterification of glycerol and dimethyl carbonate.[22] In addition, the agglomeration of ZIF-8 often occurs in the catalytic reaction due to the large specific surface area. Embedding ZIF-8 into layered hydrotalcites can not only alleviate the agglomeration of catalysts but also disperse the basic sites to avoid the by-product generation of the transesterification reaction due to excessive alkali density.[23]

ZIF-8 modified by ionic liquid [APmim]OH was designed and synthesized based on MOFs for high value-added conversion of biodiesel by-product glycerol in this paper. The alkalinity of modified ZIF-8 was increased by encapsulating aminopropyl imidazole hydroxide ionic liquid in ZIF-8. In addition, Ca–Mg–Al hydrotalcites modified by MOFs not only improved the distribution of basic centers, but also alleviated the agglomeration problem of MOFs. [APmim]OH/ZIF-8/LDH was applied to the transesterification of glycerol with dimethyl carbonate to

International Joint Research Center of Green Energy Chemical Engineering, East China University of Science and Technology, Meilong Road 130, Shanghai, 200237, China. E-mail: jyyang@ecust.edu.cn; xrxu86@ecust.edu.cn; Fax: +86 21 64252160; Tel: +86 21 64252160

† Electronic supplementary information (ESI) available. See DOI: 10.1039/d1ra08928e

prepare glycerol carbonate. The catalytic performance was evaluated by glycerol conversion and GC yield.

2 Experimental methods

2.1 Materials

All chemicals were used as received without any further purification. 1-Methylimidazole, 2-methylimidazole, Methanol (AR), 3-chloropropylamine hydrochloride (AR), dimethyl carbonate (CP) and glycerol (CP) were purchased from Aladdin Reagent Co., Ltd. $Zn(NO_3)_2 \cdot 6H_2O$, $Ca(NO_3)_2 \cdot 4H_2O$, $Mg(NO_3)_2 \cdot 6H_2O$, $Al(NO_3)_3 \cdot 9H_2O$, NaOH and Na_2CO_3 were purchased from Sinopharm Chemical Reagent Co., Ltd.

2.2 Synthesis of ZIF-8 modified by ionic liquid [APmim]OH

1-aminopropyl-3-methylimidazole hydroxide [APmim]OH (1.5 mmol) and 2-methylimidazole (40.0 mmol) were dissolved in anhydrous methanol (70 ml). The formed solution was slowly dropped into anhydrous methanol solution containing Zn $(NO_3)_2 \cdot 6H_2O$ (5.0 mmol). The mixture was stirred for 24 h and filtered. [APmim]OH/ZIF-8 can be obtained after filtering, washing by methanol and drying in the vacuum oven for 12 h. ZIF-8 can be prepared without the addition of ionic liquid.

2.3 Synthesis of hydrotalcites embedded by [APmim]OH/ZIF-8

Ca $(NO_3)_2$ (100 mmol), Mg $(NO_3)_2$ (50 mmol) and $Al(NO_3)_3$ (50 mmol) were dissolved in deionized water to prepare solution A according to 2 : 1 : 1 molar ratio of Ca^{2+}, Mg^{2+} and Al^{3+}. NaOH(400 mmol) and Na_2CO_3 (25 mmol) were dissolved in deionized water to prepare solution B according to 16 : 1 molar ratio of NaOH and Na_2CO_3. Some deionized water and [APmim]OH/ZIF-8 was added into a four-neck flask. The mixture was stirred and heated to 70 °C. Solution A and solution B were coprecipitated by double titration in the four-neck flask. The temperature of reaction system was kept 70 °C and pH was kept between 10 and 11 with stirring. The obtained white slurry was aged for 24 h in the constant temperature water bath at 70 °C after titration. [APmim]OH/ZIF-8/LDH can be obtained after filtering, washing by deionized water and drying in the vacuum oven at 80 °C for 12 h. The preparation diagram of [APmim]OH/ZIF-8/LDH was shown in Fig. 1.

2.4 Characterization methods

X-ray diffraction (XRD) patterns were recorded on RigakuD/max2550VB/PC (Rigaku International Corporation, Tokyo, Japan), using CuKα radiation ($\lambda = 0.154$ nm) at 45 kV, 100 mA.[24] X-ray photoelectron spectra (XPS) were recorded on ESCALAB 250. Quantitative analysis for surface elements of samples was performed on an Edax Falcon energy dispersive spectrometer (EDS). The morphologies of samples were observed by transmission electron microscopy (TEM) on Tecnai G2F20 S-TWIN and scanning electron microscopy (SEM) on Sigma 300. Fourier transform infrared (FT-IR) spectra of samples were recorded on Nicolet Magna-IR 550 *via* KBr pellet.[25] UV-vis diffuse reflectance spectroscopy was determined on Agilent Cary 5000

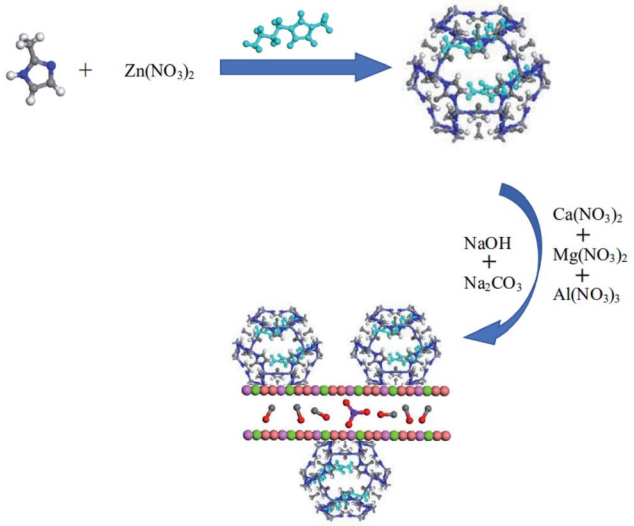

Fig. 1 Preparation diagram of [APmim]OH/ZIF-8/LDH.

spectrometer. ^{1}H NMR and ^{13}C-NMR spectra were recorded on BRUKER AVANCE III HD 400 NMR spectrometer. N_2 adsorption–desorption isotherms of the samples were recorded on Micromeritics ASAP 2460. The specific surface area was calculated by Brunauer–Emmett–Teller (BET) method. The basic strength and basic amount of samples was evaluated by Hammett titration method using 4-chloroaniline ($H_- = 26.5$), 4-nitroaniline ($H_- = 18.4$), 2.4-dinitroaniline ($H_- = 15.0$), phenolphthalein ($H_- = 9.3$) and as indicators.[26,27]

2.5 Transesterification procedure

The transesterification was conducted in a four-neck flask with the stirring device and reflux device. Glycerol and dimethyl carbonate were weighted at the molar ratio of 3 : 1 and mixed in the reactor. [APmim]OH/ZIF-8/LDH was added to catalyze the reaction of glycerol and dimethyl carbonate under N_2 atmosphere when the temperature of reaction system was heated to 75 °C. The liquid mixture can be separated from [APmim]OH/ZIF-8/LDH by centrifugation and analyzed by Jinghe GC-7860 gas chromatograph equipped with a flame ionization detector (FID) (Agilent Technologies Inc.) and a HP-PONA capillary column (50 m × 0.200 mm × 0.50 μm). Gas chromatography.[28] Programmed temperature was used to separate the different components of the vaporized mixture in the gas chromatograph.

3 3Results and discussion

3.1 Characterization of synthetic products

Synthesis and characterization details of [APmim]OH were provided in the ESI.† Fig. 2(a) displayed the X-ray diffraction patterns of ZIF-8, [APmim]OH/ZIF-8, CaMgAl-LDH and [APmim]OH/ZIF-8/LDH. The characteristic peaks of lattice planes (011), (002), (112), (022), (013) and (222) appeared in the patterns of ZIF-8 and [APmim]OH/ZIF-8, which was consistent with that reported in the literatures[29] This indicated that the

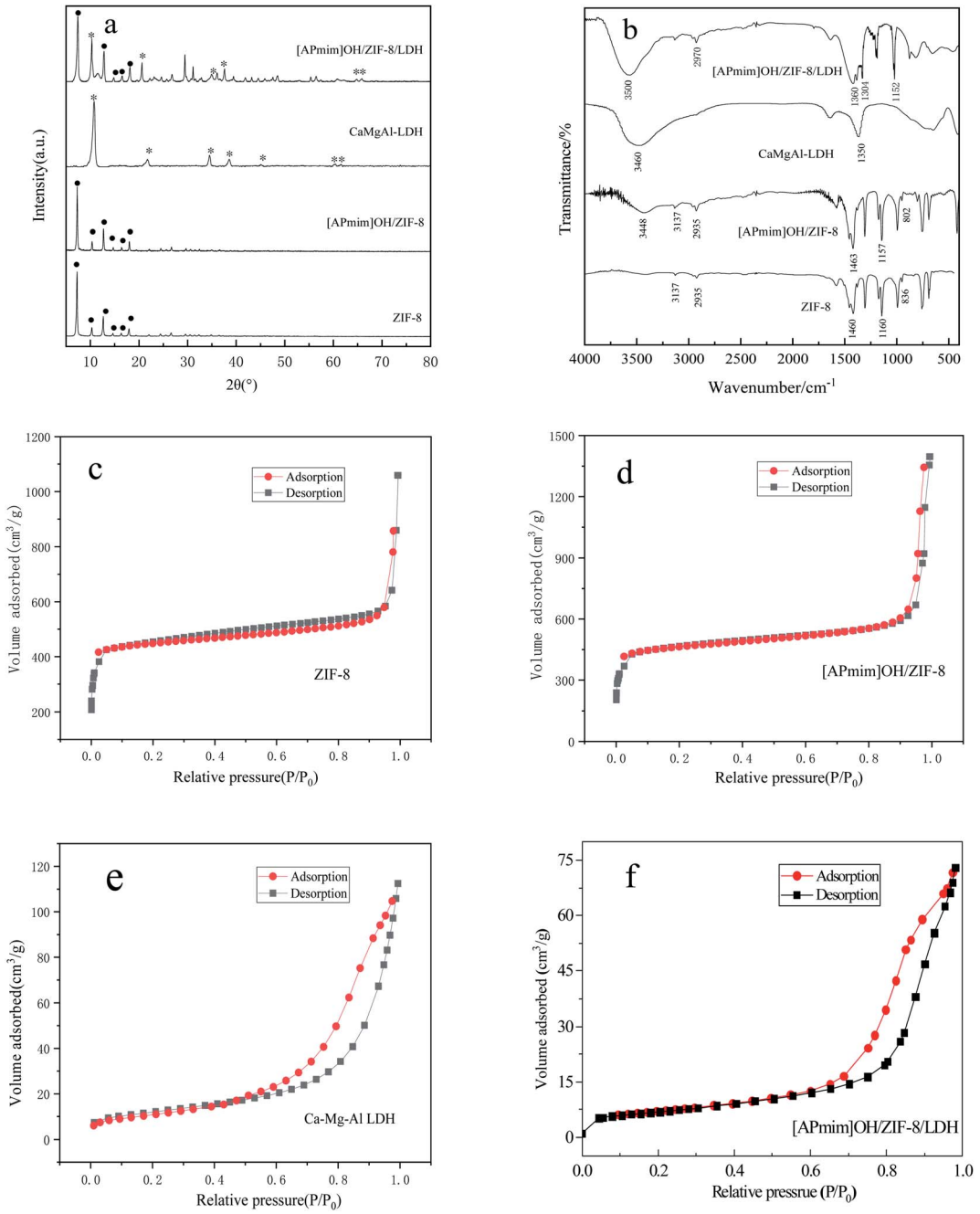

Fig. 2 XRD patterns (a), FT-IR spectra(b) and N_2 absorption isotherms (c–f) of ZIF-8, [APmim]OH/ZIF-8, CaMgAl-LDH and [APmim]OH/ZIF-8/LDH.

Table 1 Specific surface area and pore size of ZIF-8 and [APmim]OH/ZIF-8, CaMgAl-LDH and [APmim]OH/ZIF-8/LDH

Catalyst	Specific surface area ($m^2\ g^{-1}$)	Average pore size (nm)
ZIF-8	1223	1.0
[APmim]OH/ZIF-8	997	0.7
CaMgAl-LDH	102.98	17.19
[APmim]OH/ZIF-8/LDH	431.66	15.89

Table 2 Basic strength and amount of ZIF-8, CaMgAl-LDH and [APmim]OH/ZIF-8

Sample	Basic strength (H_)	Basic amount (mmol g^{-1})
ZIF-8	H_ < 9.3	0.23
[APmim]OH/ZIF-8	18.4 < H_ < 26.5	1.99
CaMgAl-LDH	9.3 < H_ < 15.0	0.50
[APmim]OH/ZIF-8/LDH	18.4 < H_ < 26.5	1.47

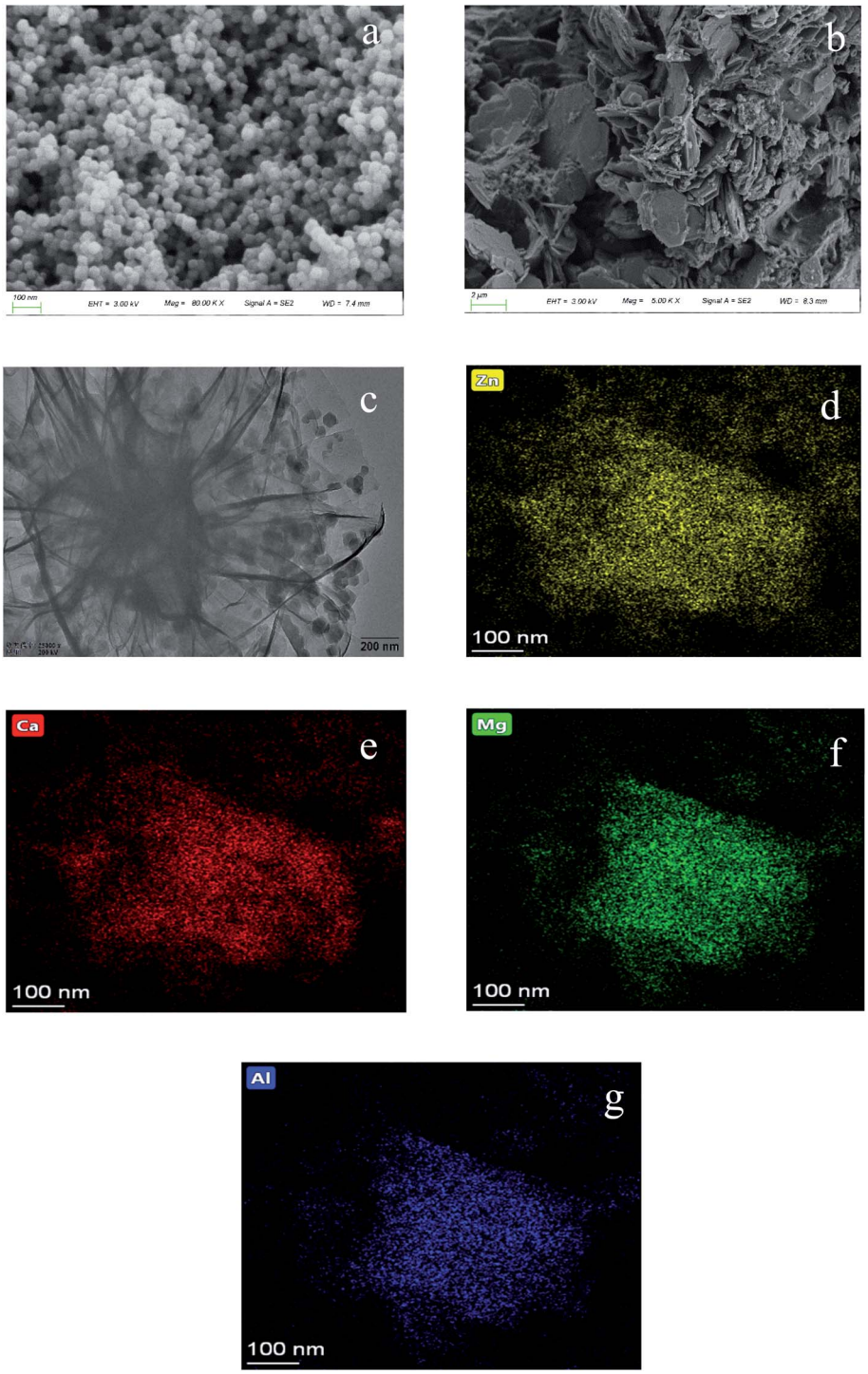

Fig. 3 SEM images of [APmim]OH/ZIF-8 (a), CaMgAl-LDH (b), TEM image of [APmim]OH/ZIF-8/LDH (c) and Zn, Ca, Mg, Al elemental mapping images of [APmim]OH/ZIF-8/LDH (d–g).

immobilization of [APmim]OH had no effect on the crystalline phase of ZIF-8. The characteristic peaks of hydrotalcites lattice planes (003), (006), (009), (015), (018), (110) and (113) appeared in the pattern of CaMgAl-LDH. The characteristic peaks of ZIF-8 and CaMgAl-LDH can be observed simultaneously in [APmim]OH/ZIF-8/LDH, which suggested that ZIF-8 had been successfully embedded into CaMgAl-LDH.

Fig. 2(b) showed the FT-IR spectra of ZIF-8, [APmim]OH/ZIF-8, CaMgAl-LDH and [APmim]OH/ZIF-8/LDH. The absorption peak at 3137 cm^{-1} was the stretching vibration peaks of unsaturated C–H bond on imidazole ring, the absorption peak at 2935 cm^{-1} was ascribed to the stretching vibration of saturated C–H bond on the imidazole branched chain, the absorption peaks at 1463 cm^{-1} and 1157 cm^{-1} were corresponded to

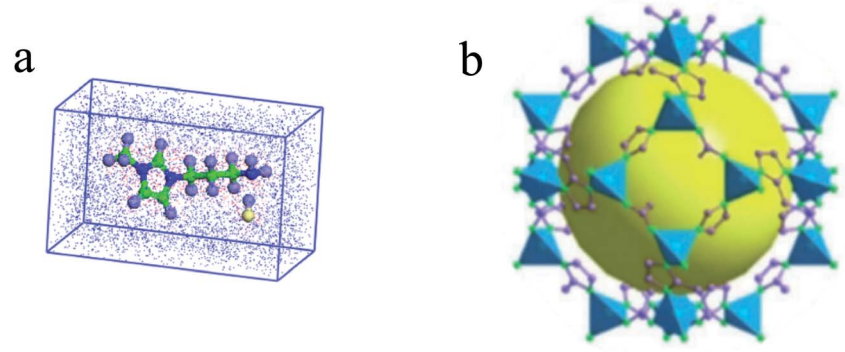

Fig. 4 Molecular diagram of [APmim]OH (a) and ZIF-8 (b).

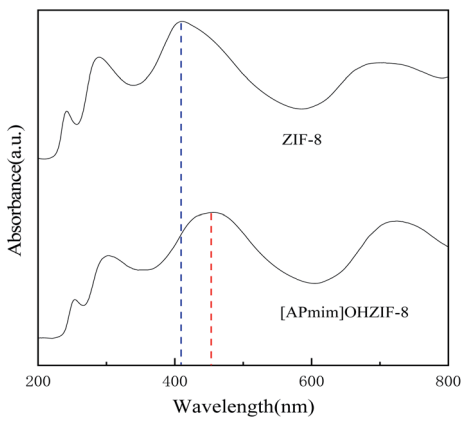

Fig. 5 UV-vis diffuse reflectance spectra of ZIF-8 and [APmim]OH/ZIF-8.

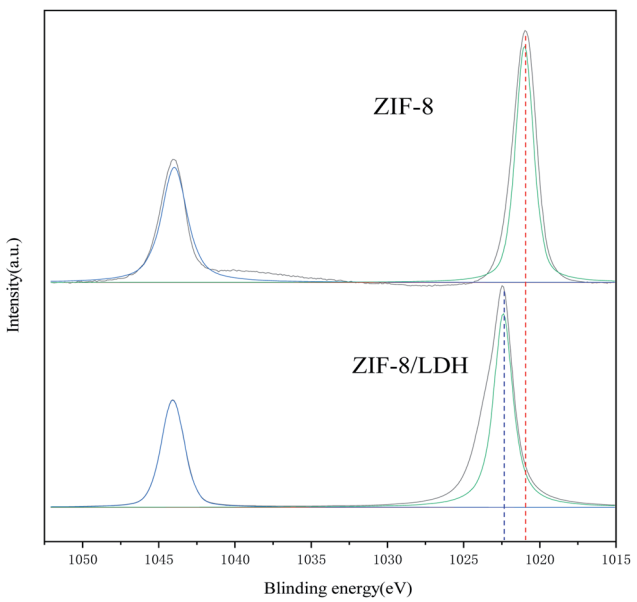

Fig. 6 XPS spectra of ZIF-8 and ZIF-8/LDH.

the stretching vibration of C–N and C=C bonds on the imidazole ring in the spectrum of ZIF-8. The obvious stretching vibration peak of hydroxyl in the ionic liquid appeared at 3448 cm^{-1} in the spectrum of [APmim]OH/ZIF-8. The out-plane bending vibration peak of N–H shifted from 836 cm^{-1} to 802 cm^{-1}, which proved that [APmim]OH had successfully coordinated with metal ions in ZIF-8.

The characteristic peaks of Ca–Mg–Al hydrotalcites were mainly the stretching vibration peak of hydroxyl at 3500 cm^{-1}, the stretching vibration peak of C–O bond related to carbonate at 1350 cm^{-1} and the stretching vibration peak caused by metal hydroxide below 1000 cm^{-1}. The adsorption peak near 2970 cm^{-1} ascribed to saturated C–H bond on the imidazole branched chain can also be found in the spectrum of [APmim]OH/ZIF-8/LDH besides the characteristic peaks similar to those of CaMgAl-LDH. The absorption peaks at 1304 cm^{-1} and 1152 cm^{-1} were corresponded to the stretching vibration of C–N and C=C bonds on the imidazole ring. It can be inferred that [APmim]OH/ZIF-8 had been successfully embedded into hydrotalcites according to the infrared spectra.

The pore structures of ZIF-8 and [APmim]OH/ZIF-8 were investigated by N_2 adsorption–desorption isotherms as shown in Fig. 2(c) and (d). The adsorption–desorption curves of ZIF-8 and [APmim]OH/ZIF-8 belonged to type I isotherm according to the IUPAC classification, indicating that the two materials were microporous. The pore size and specific surface area data of both materials were shown in Table 1. The specific surface area of ZIF-8 reached 1223 $m^2\ g^{-1}$, while the specific surface area of [APmim]OH/ZIF-8 was reduced to 997 $m^2\ g^{-1}$ due to the modification of ionic liquids.

Fig. 2(e) and (f) displayed the nitrogen adsorption–desorption isotherms of LDHs before and after modified by [APmim]OH/ZIF-8. The adsorption–desorption curves with obvious hysteresis loop belonged to type IV isotherm in the IUPAC classification, which suggested that the synthesized CaMgAl-LDH and [APmim]OH/ZIF-8/LDH was typical mesoporous materials. The specific surface area of hydrotalcites was about 102.98 $m^2\ g^{-1}$ while that of [APmim]OH/ZIF-8/LDH was 431.66 $m^2\ g^{-1}$ in Table 1 due to the high specific surface area of ZIF-8. However, the average pore size of hydrotalcites decreased from 17.19 nm to 15.89 nm after being embedded by microporous ZIF-8.

The alkalinity of ZIF-8, [APmim]OH/ZIF-8, CaMgAl-LDH and [APmim]OH/ZIF-8/LDH were characterized and the data were shown in Table 2. The basic amount of ZIF-8, [APmim]OH/ZIF-8,

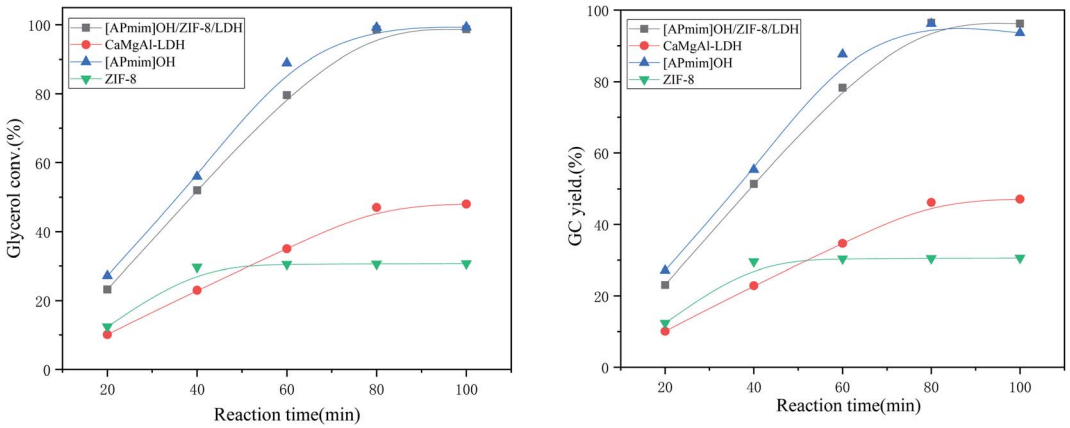

Fig. 7 Catalytic effects of CaMgAl-LDH and [APmim]OH/ZIF-8/LDH on transesterification.

CaMgAl-LDH and [APmim]OH/ZIF-8/LDH were 0.23 mmol g^{-1}, 1.99 mmol g^{-1}, 0.50 mmol g^{-1} and 1.47 mmol g^{-1} respectively. Obviously, the alkalinity of [APmim]OH/ZIF-8 and [APmim]OH/ZIF-8/LDH was strong due to the modification of alkaline ionic liquid [APmim]OH, which was conducive to the transesterification. The alkaline strength of CaMgAl-LDH was higher than ZIF-8 owing to M–OH bond in hydrotalcites.

Fig. 3 was SEM images of [APmim]OH/ZIF-8, hydrotalcites, TEM image of [APmim]OH/ZIF-8/LDH and Zn, Ca, Mg, Al elemental mapping images. The typical dodecahedral structures can be observed in SEM image of [APmim]OH/ZIF-8. The distribution of crystal particle size was relatively uniform. The SEM image of hydrotalcites displayed petal layered structures. The polygonal or circular lamellas demonstrated fine crystal morphology. The TEM images of [APmim]OH/ZIF-8/LDH showed that ZIF-8 particle was uniformly distributed on the surface of hydrotalcites lamellae. The crystal morphology of ZIF-8 was not destroyed. The even distribution of [APmim]OH/ZIF-8 in hydrotalcites can be observed from Zn Ca, Mg and Al mapping images further.

The molecule size can be calculated by Forcite module of Material Studios software. The molecule size of [APmim]OH was 4.15 Å × 4.56 Å × 8.92 Å (Fig. 4(a)), while the diameter of ZIF-8 cage was 11.6 Å (Fig. 4(b)). Thus the encapsulation of ZIF-8 in CaMgAl-LDH was reasonable in theory.

The UV-vis diffuse reflectance spectra of ZIF-8 and [APmim]OH/ZIF-8 were displayed in Fig. 5. The absorption peak of [APmim]OH/ZIF-8 was very similar to ZIF-8. The two samples had characteristic UV absorption peaks at around 420 nm. There existed red shift in the spectrum of [APmim]OH/ZIF-8 when ionic liquid [APmim]OH was encapsulated in ZIF-8 due to the charge transfer between metal and organic ligand (MLCT). The transformation of Zn (II) coordination environment led to the splitting energy change of crystal field. The characterization results proved that ionic liquids had been

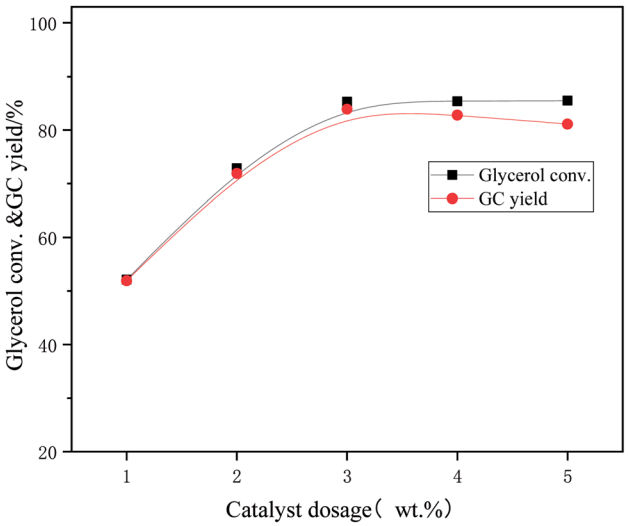

Fig. 8 Effect of catalyst dosage on glycerol conversion and GC yield.

Table 3 Comparison of [APmim]OH/ZIF-8/LDH with reported catalysts in transesterifcation of glycerol and DMC

Catalyst	Catalyst dosage (wt%)	Reaction temperature (°C)	Molar ratio of DMC to glycerol	Reaction time (min)	GC yield (%)	Ref.
Calcined dolomite	6	75	3 : 1	90	94.0	3
Na_2SiO_3-200	5	75	4 : 1	150	95.5	5
CaO/Al_2O_3	9	80	3 : 1	120	90.6	30
CaO	3	75	2 : 1	30	90.2	31
NaY zeolite	10	70	3 : 1	240	80.0	32
[APmim]OH/ZIF-8/LDH	3	75	3 : 1	80	96.5	This work

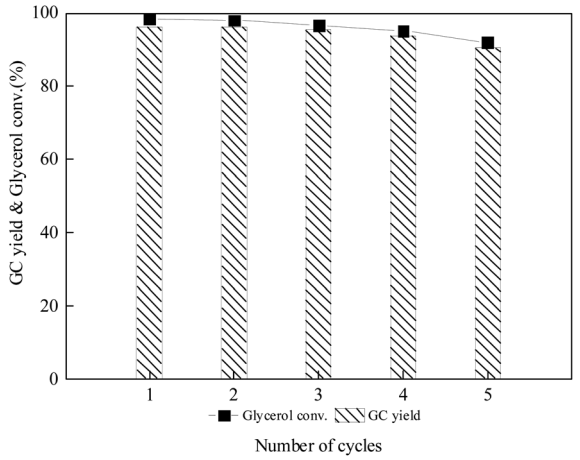

Fig. 9 Reusability of [APmim]OH/ZIF-8/LDH.

successfully encapsulated in ZIF-8 cages by coordination with metal ions, which can reduce the loss of [APmim]OH.

The chemical environment of zinc element in ZIF-8 and ZIF-8/LDH was analyzed by XPS in order to investigate the relationship between ZIF-8 and CaMgAl-LDH in ZIF-8/LDH. Fig. 6 was the XPS spectra of zinc in ZIF-8 and ZIF-8/LDH. The peak of zinc in ZIF-8/LDH shifted obviously and the electron binding energy increased compared with ZIF-8 due to the interaction between zinc ion and hydroxy in hydrotalcites. Zn–OH bond may be formed in ZIF-8/LDH, which indicated that ZIF-8 can bind with hydrotalcites stably.

3.2 Effects of [APmim]OH/ZIF-8/LDH on transesterification of glycerol and DMC

The catalytic effects of [APmim]OH/ZIF-8/LDH, [APmim]OH, ZIF-8, and CaMgAl-LDH on the transesterification of glycerol and DMC were investigated when the molar ratio of DMC and glycerol was 3 : 1 under 75 °C. The results were shown in Fig. 7. The catalytic performances of [APmim]OH/ZIF-8/LDH and [APmim]OH were much higher than the hydrotalcites and ZIF-8 since alkalinity necessary for transesterification was met. In the reaction catalyzed by [APmim]OH/ZIF-8/LDH, the glycerol conversion rate and glycerol carbonate yield at 80 min reached 98.6% and 96.5%, respectively. There was almost no change in glycerol conversion rate and glycerol carbonate yield even if the reaction continued longer. [APmim]OH encapsulated in ZIF-8 was immobilized on CaMgAl-LDH, which made the separation of ionic liquid easy and dispersed the alkaline sites to greatly reduce the side reaction. [APmim]OH raised the basicity of catalyst while ZIF-8 increased the specific surface area of catalyst. [APmim]OH/ZIF-8/LDH showed remarkable and excellent catalytic performance under the synergistic effect of ZIF-8, [APmim]OH, and CaMgAl-LDH. The catalytic performance of different catalysts was listed in Table 3.

3.3 Effects of [APmim]OH/ZIF-8/LDH dosage on transesterification of glycerol and DMC

The effect of [APmim]OH/ZIF-8/LDH dosage on the catalytic performance was investigated when the reaction temperature was 65 °C, the reaction time was 80 min, and the molar ratio of dimethyl carbonate to glycerol was 2 : 1. The experimental results were displayed in Fig. 8. The glycerol conversion increased sharply from 52.1% to 85.3% and the glycerol carbonate yield increased from 51.9% to 83.9% when the amount of catalyst increased from 1 wt% to 3 wt%, indicating that [APmim]OH/ZIF-8/LDH had excellent catalytic performance. The reaction rate and catalytic effect were significantly improved with the rise of reaction catalytic centers at this stage. However, the glycerol conversion had no detectable rise while the yield of glycerol carbonate decreased slightly when the dosage of [APmim]OH/ZIF-8/LDH mounted up further. This was mainly because excess catalyst resulted in the side reaction to generate glycidol by decarboxylation of glycerol carbonate. Moreover, massive solid catalysts intensified mass transfer resistance due to particle agglomeration thus reduced the utilization rate of catalyst. Therefore, 3 wt% can be considered as the optimal dosage of catalyst in the reaction.

3.4 Reusability test of [APmim]OH/ZIF-8/LDH

The reused performance of [APmim]OH/ZIF-8/LDH in the transesterification between dimethyl carbonate and glycerol was shown in Fig. 9. The reaction conditions were as follows: the molar ratio of DMC and glycerol was 3 : 1, the catalyst dosage was 3 wt%, the reaction temperature was 75 °C and the reaction time was 80 min. [APmim]OH/ZIF-8/LDH were recovered by filtration and washed three times with sufficient methanol then dried in the vacuum oven at 80 °C for 4 h after each reaction. The obtained solid catalyst was used in the next transesterification reaction cycle. The results showed that [APmim]OH/ZIF-8/LDH presented remarkable reusability in the catalytic reaction because the encapsulation of [APmim]OH in ZIF-8 can prevent the loss of active components effectively. There was no significant catalyst deactivation in the fifth reaction cycle and the yield of glycerol carbonate still reached 90.5%.

[APmim]OH/ZIF-8/LDH can be considered as effective catalyst for the transesterification of dimethyl carbonate with glycerol. BET analysis indicated [APmim]OH/ZIF-8/LDH with high specific surface area was beneficial to the mass transfer process in the reaction. FT-IR and XRD analysis showed that [APmim]OH, ZIF-8, and CaMgAl-LDH maintained their own characteristics in the catalyst. [APmim]OH met the alkalinity requirement of transesterification and ZIF-8 increased the specific surface area of catalyst. The interaction of [APmim]OH, ZIF-8, and CaMgAl-LDH observed in XPS and DRS UV-vis spectra enabled active components to combine with the carriers stably, thus [APmim]OH/ZIF-8/LDH presented excellent catalytic ability and reusability.

4 Conclusion

ZIF-8 modified by ionic liquid was synthesized and dispersed evenly in the CaMgAl hydrotalcites to prepare [APmim]OH/ZIF-8/LDH in this paper. The catalyst was used for transesterification of dimethyl carbonate with glycerol to prepare

glycerol carbonate. The strong basicity of [APmim]OH was beneficial for the transesterification reaction. Dispersing [APmim]OH/ZIF-8 in hydrotalcites can not only enhance the alkaline strength of catalyst, but also avoid the agglomeration of ZIF-8. In addition, the increased specific surface area of hydrotalcites due to the intercalation of ZIF-8 significantly raised the collision probability between active sites and reactants. The glycerol conversion rate can still reach more than 90% after being reused five times because the encapsulation of [APmim]OH in ZIF-8 reduced the leaching of active components. Therefore, [APmim]OH/ZIF-8/LDH presented tremendous application value in industry because of the remarkable catalytic ability and reusability.

Conflicts of interest

There are no conflicts to declare.

References

1 A. S. Yusuff, A. O. Gbadamosi and L. T. Popoola, Biodiesel production from transesterified waste cooking oil by zinc-modified anthill catalyst: Parametric optimization and biodiesel properties improvement[J], *J. Environ. Chem. Eng.*, 2021, **9**(2), 104955.

2 J. Huang, Y. Zou and M. Yaseen, Fabrication of hollow cage-like CaO catalyst for the enhanced biodiesel production *via* transesterification of soybean oil and methanol[J], *Fuel*, 2021, **290**, 119799.

3 Y. T. Algoufi, G. Kabir and B. H. Hameed, Synthesis of Glycerol Carbonate from Biodiesel By-Product Glycerol over Calcined Dolomite[J], *J. Taiwan Inst. Chem. Eng.*, 2017, **70**, 179–187.

4 K. Shikhaliyev, P. U. Okoye and B. H. Hameed, Transesterification of Biodiesel Byproduct Glycerol and Dimethyl Carbonate over Porous Biochar Derived from Pyrolysis of Fishery Waste[J], *Energy Convers. Manage.*, 2018, **165**, 794–800.

5 S. Wang, P. Hao, S. Li, A. Zhang, Y. Guan and L. Zhang, Synthesis of Glycerol Carbonate from Glycerol and Dimethyl Carbonate Catalyzed by Calcined Silicates[J], *Appl. Catal., A*, 2017, **542**, 174–181.

6 X. Song, Y. Wu, F. Cai, D. Pan and G. Xiao, High-efficiency and low-cost Li/ZnO catalysts for synthesis of glycerol carbonate from glycerol transesterification: The role of Li and ZnO interaction[J], *Appl. Catal., A*, 2017, **532**, 77–85.

7 G. Parameswaram, M. Srinivas, B. Hari Babu, *et al.*, Transesterification of glycerol with dimethyl carbonate for the synthesis of glycerol carbonate over Mg/Zr/Sr mixed oxide base catalysts[J], *Catal. Sci. Technol.*, 2013, **3**(12), 3242–3249.

8 P. U. Okoye, A. Z. Abdullah and B. H. Hameed, Stabilized Ladle Furnace Steel Slag for Glycerol Carbonate Synthesis *via* Glycerol Transesterification Reaction with Dimethyl Carbonate[J], *Energy Convers. Manage.*, 2017, **133**, 477–485.

9 A. Poungsombate, T. Imyen and P. Dittanet, Direct synthesis of dimethyl carbonate from CO2 and methanol by supported bimetallic Cu–Ni/ZIF-8 MOF catalysts[J], *J. Taiwan Inst. Chem. Eng.*, 2017, **80**, 16–24.

10 M. S. Khayoon and B. H. Hameed, Mg1+xCa1-x as reusable and efficient heterogeneous catalyst for the synthesis of glycerol carbonate *via* the transesterification of glycerol with dimethyl carbonate[J], *Appl. Catal., A*, 2013, **466**, 272–281.

11 S. E. Kondawar, C. R. Patil and C. V. Rode, Tandem Synthesis of Glycidol *via* Transesterification of Glycerol with DMC over Ba-Mixed Metal Oxide Catalysts[J], *ACS Sustainable Chem. Eng.*, 2017, **5**(2), 1763–1774.

12 J. Gao, Y. Wang and H. Wu, Construction of a sp3/sp2 Carbon Interface in 3D N-Doped Nanocarbons for the Oxygen Reduction Reaction, *Angew. Chem.*, 2019, **131**, 15233–15241.

13 W. Ying, J. S. Cai and K. Zhou, Ionic Liquid Selectively Facilitates CO2 Transport through Graphene Oxide Membrane, *ACS Nano*, 2018, **12**, 5385–5393.

14 C. X. Miao, H. F. Zhuang and Y. T. Wen, Efficient thiolation of alcohols catalyzed by long chained acid-functionalized ionic liquids under mild conditions, *Eur. J. Org. Chem.*, 2019, **19**, 3012–3021.

15 X. J. Wei, H. B. Li and Q. H. Zhang, A selective control of volatile and non-volatile superconductivity in an insulating copper oxide *via* ionic liquid gating, *Sci. Bull.*, 2020, **65**, 1607–1613.

16 L. Zheng, J. Li and M. M. Yu, Molecular sizes and antibacterial performance relationships of flexible ionic liquid derivatives, *J. Am. Chem. Soc.*, 2020, **142**, 20257–20269.

17 W. Ren, X. Tan and X. Chen, Confinement of Ionic Liquids at Single-Ni-Sites Boost Electroreduction of CO2 in Aqueous Electrolytes[J], *ACS Catal.*, 2020, **10**, 13171–13178.

18 Y. Zheng, L. Zhang and H. Huang, ZIF-67-derived Co, Ni and S co-doped N-enriched porous carbon polyhedron as an efficient electrocatalyst for oxygen evolution reaction (OER) [J], *Int. J. Hydrogen Energy*, 2019, **44**, 27465–27471.

19 Xu Jiang, S. Li and Y. Bai, Ultra-facile aqueous synthesis of nano porous zeolitic imidazolate framework membranes for hydrogen purification and olefin/paraffin separation[J], *J. Mater. Chem. A*, 2019, **7**, 10898–10904.

20 W. Zhang, L. Zong and S. Liu, An electrochemical sensor based on electro-polymerization of caffeic acid and Zn/Ni-ZIF-8–800 on glassy carbon electrode for the sensitive detection of acetaminophen[J], *Biosens. Bioelectron.*, 2019, **131**, 200–206.

21 B. Joshi, E. Samuel and H. S. Jo, Hierarchically designed ZIF-8-derived Ni@ZnO/carbon nanofiber freestanding composite for stable Li storage[J], *Chem. Eng. J.*, 2018, **351**, 127–134.

22 W. L. Xue, W. H. Deng and H. Chen, MOF-Directed Synthesis of Crystalline Ionic Liquids with Enhanced Proton Conduction[J], *Angew. Chem. Int. Ed.*, 2020, **59**, 2–10.

23 X. Zhang, T. Zhang and Y. Wang, Mixed-matrix membranes based on Zn/Ni-ZIF-8-PEBA for high performance CO2 separation[J], *J. Membr. Sci.*, 2018, **560**, 38–46.

24 G. Liu, J. Yang and X. Xu, Synthesis of Hydrotalcites from Waste Steel Slag with [Bmim]OH Intercalated for the

Transesterification of Glycerol Carbonate[J], *Molecules*, 2020, **25**(19), 4355.

25 W. Bing, H. Wang, Z. Lei, *et al.*, CaMnAl-hydrotalcite solid basic catalyst toward aldol condensation reaction with a comparable level to liquid alkali catalysts[J], *Green Chem.*, 2018, **20**, 3071–3080.

26 Y. Wang, W. Y. Huang, Y. Chun, *et al.*, Dispersion of potassium nitrate and the resulting strong basicity on zirconia[J], *Chem. Mater.*, 2001, **13**, 670–677.

27 W. Xie and H. Li, Alumina-supported potassium iodide as heterogeneous catalyst for biodiesel production from soybean oil[J], *J. Mol. Catal. A: Chem.*, 2006, **255**(1), 1–9.

28 G. Liu, J. Yang and X. Xu, Synthesis of hydrotalcite-type mixed oxide catalysts from waste steel slag for transesterification of glycerol and dimethyl carbonate[J], *Sci. Rep.*, 2020, **10**, 10273.

29 S. R. Venna, J. B. Jasinski and M. A. Carreon, Structural Evolution of Zeolitic Imidazolate Framework-8[J], *J. Am. Chem. Soc.*, 2010, **132**(51), 18030–18033.

30 P. Lu, H. Wang and K. Hu, Synthesis of glycerol carbonate from glycerol and dimethyl carbonate over the extruded CaO-based catalyst[J], *Chem. Eng. J.*, 2013, **228**, 147–154.

31 O. G. José, G. J. A. Olga and M. M. Belén, Synthesis of glycerol carbonate from glycerol and dimethyl carbonate by transesterifcation: Catalyst screening and reaction optimization[J], *Appl. Catal., A*, 2009, **366**, 315–324.

32 S. Pan, L. Zheng and R. Nie, Transesterifcation of glycerol with dimethyl carbonate to glycerol carbonate over Na-based zeolites[J], *Chin. J. Catal.*, 2012, **33**, 1772–1777.